Extended abstract
13th Conf. of IOAS-AOLS
AMS Meetings 2008

6.4. Multi-scale Analysis and Prediction of the 8 May 2003 Oklahoma City Tornadic Supercell Storm Assimilating Radar and Surface Network Data using EnKF

Ting Lei[1]*, Ming Xue[1,2] and Tianyou Yu[3,4]
[1]Center for Analysis and Prediction of Storms
[2]School of Meteorology
[3]School of Electronic and Computing Engineering
[4]Atmospheric Radar Research Center
University of Oklahoma

1. Introduction

Ensemble Kalman filter (EnKF) is an emerging advanced method that can be applied to storm-scale atmospheric data assimilation. Since its rather successful use in observation system simulation experiments (OSSEs, e.g., Snyder and Zhang 2003; Zhang et al. 2004; Tong and Xue 2005; Xue et al. 2006) at the convective storm scale, much efforts has been made to apply it to real cases (Dowell et al. 2004; Dowell and Wicker 2004; Wicker and Dowell 2004; Tong 2006; Dowell and Wicker 2009). The OSSEs usually assume a perfect prediction model and a perfect storm environment, when the same model and the same environmental sounding are used for both truth simulation and in data assimilation and their results are nearly perfect. The results of real data cases are, however, far from perfect. In fact, of the storm-scale structures are analyzed quite well in these cases, but the ensuing forecasts deteriorate quickly, within tens of minutes.

With real data cases, there are of course many more sources of error. The prediction model is definitely not perfect; in fact, there are a lot of uncertainty with the drop-size distribution of the cloud and hydrometeor species within microphysics parameterization alone to which the storm prediction can be very sensitive (Snook and Xue 2008; Tong and Xue 2008a; Dawson et al. 2009). The storm environment often defined using a single sounding or through mesoscale analysis, can also contain significant error. In such a case, even if the storm itself is analyzed perfectly using EnKF and radar data, the prediction can quickly deteriorate because it is known that the environmental wind and thermodynamic profiles have a strong control on storm dynamics (e.g., Weisman and Klemp 1982). Other issues and uncertainties that are difficult to deal with in real data cases include insufficient data coverage, unknown, uncorrected or poorly characterized observation errors, possible observation error correlation, and improper tuning of the EnKF algorithms (including covariance inflation and location) due to the lack of truth information as a guide. All these make the real data assimilation and prediction at the storm-scale much more challenging than working with OSSEs, where errors in both data and model can be well understood, and a complete truth is available for verification.

To improve the EnKF analysis and subsequent forecast for thunderstorms, all of the above issues have to be addressed. The model error issue needs to be addressed by using more accurate model physics and increased resolution (e.g., Dawson et al. 2009), and/or through simultaneous state and error estimation (e.g., Tong and Xue 2008b), and by adequately accounting for remaining model error via ideally adaptive ensemble covariance inflation (e.g., Anderson 2008). The uncertainty of the storm environmental needs to be reduced by assimilating all other available observations, including those from rawinsonde, wind profiler, aircraft, and mesoscale surface networks. The EnKF data assimilation system needs to be improved or fine tuned so that the ensemble-derived background error covariance adequate reflects the scale and magnitude of the error. Flow-dependent covariance inflation and localization (e.g., Anderson 2007) may be necessarily, especially in such cases where the scales, magnitudes and growth rates in convective and non-convective regions can be rather different. Different techniques (e.g., multiplicative, additive, adjustment or model perturbation methods) and/or their combinations may have to be employed for optimal covariance inflation, and for specifying the initial ensemble perturbations.

This paper represents one of our efforts working towards improving thunderstorm data assimilation and prediction with a real data case via EnKF. More specifically, the ARPS (Advanced Regional Prediction System, Xue et al. 2003) EnKF system (Tong and Xue 2005; Xue et al. 2006) is enhanced and applied to the 8 May 2003 Oklahoma City tornadic supercell storm case, for the assimilation of data from WSR-88D radars and high-resolution surface networks. The latter include the Oklahoma Mesonet with data available every 5 minutes.

To be able to handle data and flow features at both mesoscale and storm scale, two one-way nested ensemble data assimilation systems are used, with a 1 km horizontal-resolution system nested inside a larger 3-km system. Perturbations representative of mesoscale forecast errors are generated by analyzing perturbed pseudo soundings extracted from the first guess using the

* *Corresponding author address: Dr. Ting Lei, CAPS, University of Oklahoma, 120 David Boren Blvd, Norman OK 73072. e-mail: tlei@ou.edu.*

ARPS 3DVAR. Such perturbed analyses become the initial conditions of the 3-km ensemble. A similar procedure is used to construct perturbed boundary conditions for the 3-km system, which assimilates conventional observations, including surface mesonet data.

The nested storm-scale EnKF system starts from the 3-km ensemble at a later time, and assimilates additional level-II WSR-88D radar data at 5-minute intervals. Storm-scale perturbations are introduced into the initial conditions of this ensemble. Various inflation techniques are tested on the high-resolution grid. The results of both the analyses and subsequent forecasts will be presented. The forecasts will be directly verified against radar observations.

The 8 May 8 2003 case is chosen because it is an isolated supercell case that produced F-4 intensity tornadoes in Moore, Oklahoma, between Oklahoma City (OKC) and Norman, and the storm was well captured by the OKC WSR-88D radar (KTLX), as well as the OKC airport TDWR and the experimental dual-polarization WSR-88D radar at Norman (KOUN). The storm is also covered by other surrounding WSR-88D radars, including that from Frederick in southwest Oklahoma (KFRD). Several earlier studies on this case already exist, including the rather successful efforts of Hu and Xue (2007a; 2007b) that assimilated KTLX data using the ARPS 3DVAR and cloud analysis package using frequent intermittent assimilation cycles. Natenberg (2008) and Natenberg and Gao (2008) further showed that by using data from all available radars, a single-time analysis using the ARPS 3DVAR and cloud analysis procedure is able to provide an initial condition that results in a reasonable prediction up to one hour. Preliminary efforts applying EnKF to this case by Dowell and Wicker (2004) and Wicker and Dowell (2004) were less that satisfactory with the prediction, while Dowell and Wicker (2009) presents only the analysis results, where additive noise is used to improve the EnKF analysis of this storm.

In this paper, through multi-scale EnKF analysis that includes both radar and high-frequency surface observations, and by tuning the EnKF algorithm, storm forecasts at 1 km and 500 m horizontal resolutions are obtained that are believed to be better than earlier results. The predicted storm maintains its intensity as well as strong low-level rotation characteristics that are consistent with observations for over 1 hour.

The rest of this paper is organized as follows. Section 2 describes radar data preprocessing procedure, the surface observation operator incorporated into the EnKF system, the multiscale analysis procedure. Section 3 presents the experiment setup and section 4 the results. Section 5 draws conclusions and includes some further discussions.

2. Multiscale EnKF analysis system

The ARPS EnKF system is used in this study. The system can assimilate radar data (radial velocity and reflectivity) pre-processed to three different coordinates: 1) at the model grid points (as in Tong and Xue 2005), 2) on the radar elevation levels but in the horizontal directions on the model Cartesian grid (as in Xue et al. 2006), and 3) in the original radar coordinates (as in Lei et al. 2008). In this study, the second approach is used.

2.1. Radar data preprocessing

In this work, the 88d2arps program is modified to put data on the elevation levels and used to preprocess the level-II data from KTLX radar for use by ARPS EnKF. Quality control, including radial velocity dealiasing and despecle for both radial velocity and reflectivity are included (for specifics, refer to Brewster et al. 2005). Using Cressman objective analysis method, raw observations are processed at each elevation level to the intersecting points of the tilts with model grid columns. A time interpolation is then performed between the same elevations of two consecutive scan volumes to bring the data to the analysis times that are 5 min apart. The error standard deviations for the radial velocity and reflectivity data are assumed to be 2 m s^{-1} and 4 dBZ, respectively, in the data assimilation.

2.2. EnKF analysis of surface observations

The assimilation of frequent surface observations is believed to be important for improving the storm environment. EnKF assimilation of surface observations for mesoscale prediction has been reported in recent studies (e.g., Fujita et al. 2007; Stensrud et al. 2008). The assimilation of hourly routine surface data was found to improve subsequent mesoscale forecasts. Dong et al. (2007) investigated the impact of simulated high-resolution surface data at 5 min intervals on the analysis and prediction of a supercell storm. It was found that the surface data are especially valuable when the radar is located at a distance from the storm, so that low-level radar data coverage is missing. The quality of analysis is found to continue to increase as the network density increases. In that OSSE study, the surface observations are assumed to be available at the lowest model level so that no interpolation is needed in the vertical. Linear interpolation is performed in the horizontal to project the grid point values to the station locations as part of the observation operator.

Because the first model level is usually not at the station level (AGL), and significant vertical gradient often exists near the surface, more sophisticated treatment in the observation operators in brining the model state to the station level is desirable.

In this work, surface observation operator is improved by using interpolation based on the surface layer profiles based on Byun (1990).

For stable conditions, Monin-Obukhov stability parameter ζ used in the profiles is given by

$$\zeta = \frac{-(2\beta_h Ri_b - 1) - \{1 + [4(\beta_h - \beta_m) Ri_b / \Pr]\}^{1/2}}{2\beta_h(\beta_m Ri_b - 1)},$$

For unstable conditions:

When $Ri_b \geq -0.2097$,

$$\zeta = \left(\frac{z}{z - z_0}\right) \ln\left(\frac{z}{z_0}\right)\left[-2\sqrt{Q_b}\cos\left(\frac{\theta_b}{3}\right) + \frac{1}{3\gamma_m}\right].$$

When $-0.2097 < Ri_b \leq 0$

$$\zeta = \left(\frac{z}{z - z_0}\right) \ln\left(\frac{z}{z_0}\right)\left[-\left(T_b + \frac{Q_b}{T_b}\right) + \frac{1}{3\gamma_m}\right].$$

Where, Ri_b is the bulk Richardson number

$$Ri_b = \frac{g}{0.5(\theta_1 + \theta_s^{extr})}\left(\frac{(\theta_1 + \theta_s^{extr})}{U_1^2}\right).$$

$$\Pr = 0.74,\ s_b = \frac{Ri_b}{\Pr},\ Q_b = \frac{1}{9}\left[\frac{Ri_b}{\gamma_m^2} + 3\frac{\gamma_h}{\gamma_m}s_b^2\right]$$

$$P_b = \frac{1}{54}\left[-\frac{1}{\gamma_m^3} + \frac{9}{\gamma_m}\left(-\frac{\gamma_h}{\gamma_m} + 3\right)s_b^2\right]$$

$$\theta_b = \arccos\left[\frac{P_b}{\sqrt{Q_b^3}}\right]$$

$$T_b = \left(\sqrt{P_b^2 - Q_b^3} + |P|\right)^{1/3}$$

When the Monin-Obukhov stability parameter ζ is specified, the model version of the 10-m wind and 2-m temperature can be determined from the values at the lowest model level according to the corresponding similarity functions (Eqs. 10 and 11 in Byun 1990). In this work, the lowest grid level for all model variables except for vertical velocity is at about 10 m AGL hence this procedure is less important for wind than to temperature and moisture. The surface pressure is calculated from the lowest level above ground according to hydrostatic balance. Surface water vapor mixing ratio, q_v, is calculated by assuming that station dew point temperature is equal to that at the lowest model level. A similarity-theory based processing is also performed in Fujita et al. (2007) in their EnKF assimilation of surface data for mesoscale predictions.

2.3. Multiscale EnKF analysis

As in our earlier studies, the sequential ensemble square-root filter (EnSRF) algorithm after Whitaker and Hamill (2002) is used. As briefly described in Introduction, we use two one-way nested grids at 3 and 1 km horizontal resolutions for the EnKF analysis and forecast.

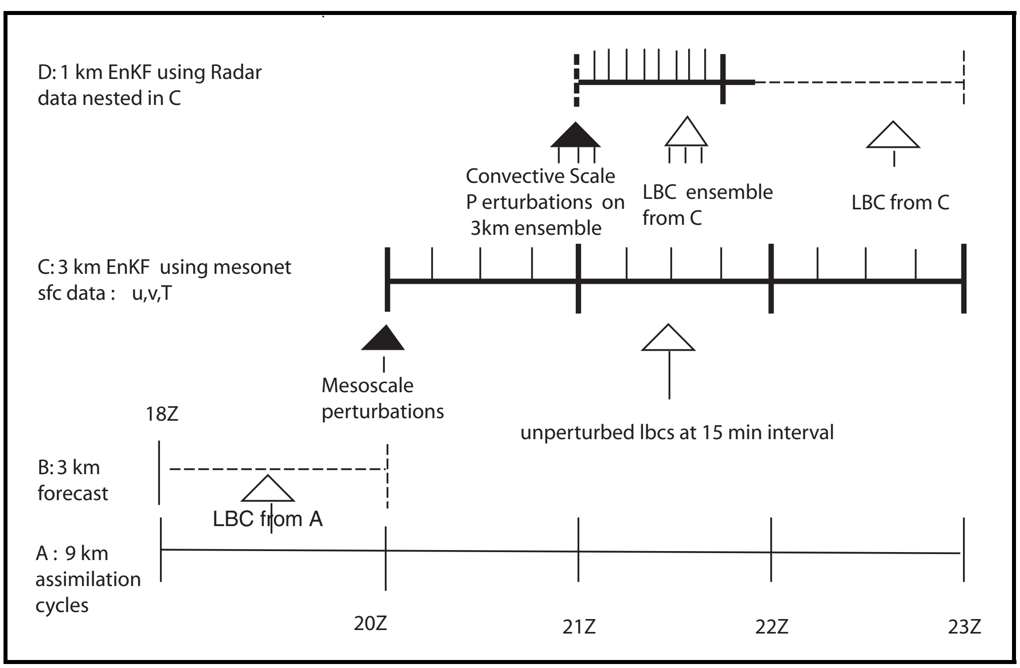

Fig. 1 . Diagram for multiscale analysis procedure.

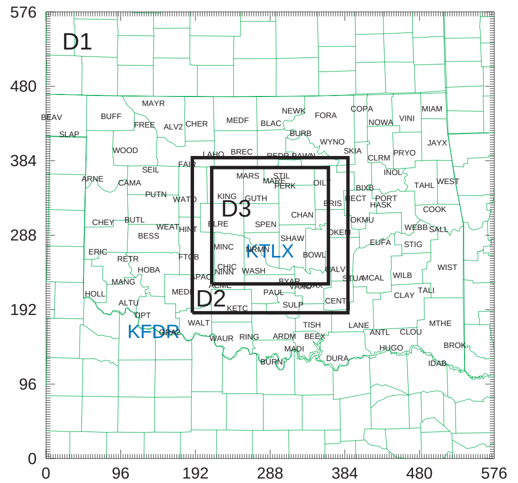

Fig. 2. D1 is the domain of horizontal resolution 3 km, D2 the domain of 1 km resolution and D3 is the domain for forecast at 500 m horizontal resolution. Mesonet stations and KTLX and KFDR radars are also labeled.

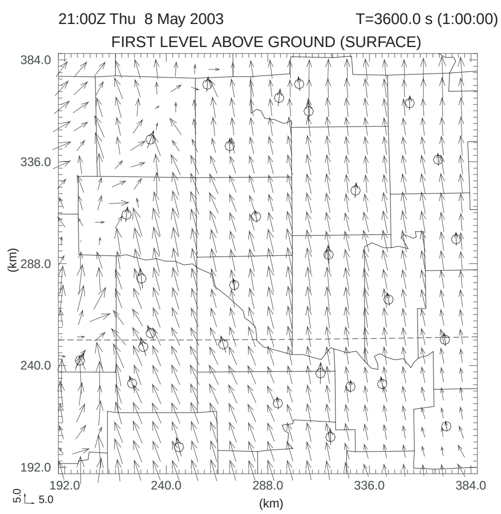

Fig. 3. The ensemble mean analysis of wind vectors from 3 km EnKF, at 10 m AGL and 2100 UTC, plotted in the 1 km domain. Vectors with circles are Mesonet observations, that indicate the match of the analysis to observations.

The 3 km grid provides an ensemble of analyses (during its assimilation period) and forecasts that provides the lateral boundary conditions (LBCs) with mesoscale variability for the 1 km grid. Boundary conditions with dynamically consistent perturbations are considered important for properly maintaining spread within the nested ensemble (Nutter et al. 2004). The 3 km system also acts to provide an initial ensemble for starting the EnKF cycles on the 1 km grid. The EnKF analyses on the outer grid are also expected to bring in mesoscale observational information and help improve the storm environment on the fine grid.

Figure 1 shows the schematic of the assimilation and forecast configurations for our control experiment. Because the main goal of the 3 km grid is mesoscale data assimilation and prediction, we do not assimilate radar data on this grid. Hourly analyses between 1800 UTC, 8 May and 0000 UTC 9 May, 2003, obtained using the ARPS 3DVAR on a 9 km grid, as described in Hu and Xue (2007a), are used to provide unperturbed LBCs to the 3 km ensemble. Given that the 3 km grid is sufficiently large, the lack of perturbations in the 3 km LBCs does not appear to affect our 1 km domain within the time range of interest.

As shown in Fig. 1, a single pre-forecast is first performed on the 3 km grid from 1800 to 2000 UTC, starting from interpolated 9 km analysis at 1800 UTC. The 2 hour forecast valid at 2000 UTC is used as the background for a set of 3DVAR analyses on the 3 km grid to produce perturbed initial conditions for the 3 km ensemble.

To initialize the 3-km ensemble, perturbations aimed at sampling mesoscale uncertainty are introduced. The approach taken here is a modified perturbed observation method. At this non-synoptic time for our relatively small grid, the predominant form of observations is surface observations, including those from the Oklahoma Mesonet. As mentioned earlier, radar data are not used on this grid.

To sample mesoscale uncertainties, we extract 10 pseudo sounding profiles from the analysis background, adding to them Gaussian-distributed random perturbations with sizes typical of rawinsonde observation error. We further add perturbations to the real surface observations of sizes typically of surface observation error. These perturbed real and pseudo observations are then analyzed using the ARPS 3DVAR in two separate passes, using horizontal error de-correlation scales comparable to the mean network spacing of each type of observations. The 3DVAR analysis is performed N number of times, where N is the number of ensemble members in the follow-on EnKF analysis. $N = 40$ in our case. Different realizations of random perturbations were added to the observations used in each analysis. Because the 3DVAR background error covariance is used in the analysis, the perturbation fields of the resulting analyses should have structures reflecting such covariance structures. It should be noted that in the absence of real observations, the pseudo soundings will have no effect if no perturbations are added to them, i.e., the analysis increments will be zero and all analyses will be the same in that case. The noise added to the observations introduces perturbations into the analyses that are smoothed to the scale of background error covariance by the 3DVAR analysis.

Starting from the set of perturbed initial conditions, the first forecast cycles are launched on the 3 km grid. Fifteen-minute-long EnKF analysis cycles are performed on this grid through 2300 UTC, analyzing Oklahoma Mesonet and other surface observations; this set of ensemble analyses provides LBCs for the EnKF analysis and forecast on the nested 1 km grid (Fig. 1).

To initialize the 1 km EnKF analysis cycles, the 3 km ensemble analyses are interpolated to the 1 km grid at 2100 UTC. Additional storm-scale perturbations are then added to these analyses on the 1 km grid, and the perturbations are generated by applying a smoothing procedure on random perturbations, as described in Tong and Xue (2008a). The EnKF analysis cycles are then started on the 1 km grid, and radar data are assimilated every 5 minutes.

In the control experiment to be discussed in this paper, in the 3 km EnKF, only *u*, *v*, and T observations of Oklahoma Mesonet are analyzed, at 15 min intervals from 2015 to 2300 UTC. The surface observation errors are specified as 1 m s^{-1} for the wind components and 1.11 K for temperature. No covariance inflation is applied in the 3 km EnKF. The covariance localization radius in the horizontal direction is 50 km and 4 km in the vertical direction. Fig. 3 shows the ensemble mean surface wind vectors of the 3 km EnKF analysis at 2100 UTC, plotted on the 1 km grid.

A number of experiments have been performed that vary in configuration details. In this paper, we will only report on results of the control experiment, in which the 1 km EnKF analyses end at 2155 UTC, and forecasts starting from the ensemble mean analysis at the 1 km grid as well as on an enhanced 500 m grid (see Fig. 2) are run up to 2300 UTC. Between 2210 and 2240 UTC, a tornado of F-4 intensity formed in the real storm (Hu and Xue 2007a).

In the 1 km EnKF analyses, multiplicative inflation is applied throughout the domain with a coefficient of 1.02. The covariance localization radius is 6 km in the horizontal and 4 km in the vertical. All reflectivity data are used, including those that show no precipitation. For radial velocity, only those with reflectivity larger than 10 dBZ are used. In the control experiment, data from KTLK and KFRD radars are assimilated.

For both 3 and 1 km grids, the ARPS was configured with 50 vertical levels with a minimum vertical grid spacing of 20 m at the surface. Physics options including the 1.5-order TKE subgrid-scale turbulence, Lin ice microphysics, complete long and short wave radiation, and a two-layer soil model predicting the land surface conditions (for details see Xue et al. 2001).

3. Results.

For comparison purpose, we first present in Fig. 4 the KTLX-observed reflectivity, at its lowest elevation of 0.48º, at the end time of 1 km EnKF cycles and at later forecast times. During this period, a supercell is prominent near the center of domain, and at 2155 UTC, the southwestern tip of the core reflectivity region is at the northwest tip of Cleveland County (the one with triangular shape at the domain center). This cell propagated steadily north-northeastward, and developed a hook echo pattern by 2210 UTC (Fig. 4c). In fact, this is the time the long-track F4-intensity tornado first touched down. A hint of hook echo pattern is evident throughout this period.

At 2511 UTC, a weak cell is found in the southwestern part of this domain, and this cell reached it maximum echo intensity at around 2220 UTC (Fig. 4d) then decayed over the next twenty minutes.

Fig. 5a shows the final ensemble mean analysis at 2155 UTC, obtained on the 1 km grid. The model reflectivity fields are projected to the same 0.48º elevation of KTLX radar for direct comparison. It can be seen that the general pattern of the analyzed reflectivity agrees with that observed, for both the main supercell and the small developing cell in the southwest. The main discrepancy lies with the reflectivity on the northside of the core reflectivity, which is actually associated with a cell split from the main one. This part of analyzed reflectivity is weaker than observed.

In the ensuing forecast, the predicted main cell maintains its intensity and propagates at a similar speed and direction as observed, with a slight southward track error by the end of the forecast at 2300 UTC (compare Fig. 5h with Fig. 4h). The reflectivity associated with the main cell has a generally similar pattern to observations. One obvious problem with the forecast is the continued growth of the cell to the southwest, which moves to the east of Cleveland County by 2300 UTC while in reality it has died by this time. It is not clear why this storm behaved incorrectly in the model; most likely the model predicted storm environment in this region is unduly favorable for the continued intensification of this cell. Fortunately, this over-grown cell did not significantly interfere with the main cell up to the end of our forecast.

From Fig. 5, we can see that during the initial period of forecast, the main cell did develop a hook echo structure. This is evident at 2200, just 5 minutes into the forecast (Fig. 5b). By 2210 (Fig. 5c), the hook becomes less clear although strong rotation exists as seen from zoomed plots (not shown). In the mean time, the rotational characteristics in the reflectivity field do appear somewhat weak, and we suspected that this is related to the grid resolution. While 1 km horizontal resolution can resolve the supercell storm, smaller scale structures, including the low-level rotation, can be easily underpredicted. To test this hypothesis, we interpolated the final 1 km EnKF ensemble-mean analysis at 2155 UTC to a slightly smaller 500 m resolution grid (see Fig. 1), and produced forecast for the same length. The corresponding reflectivity fields are shown in Fig. 6.

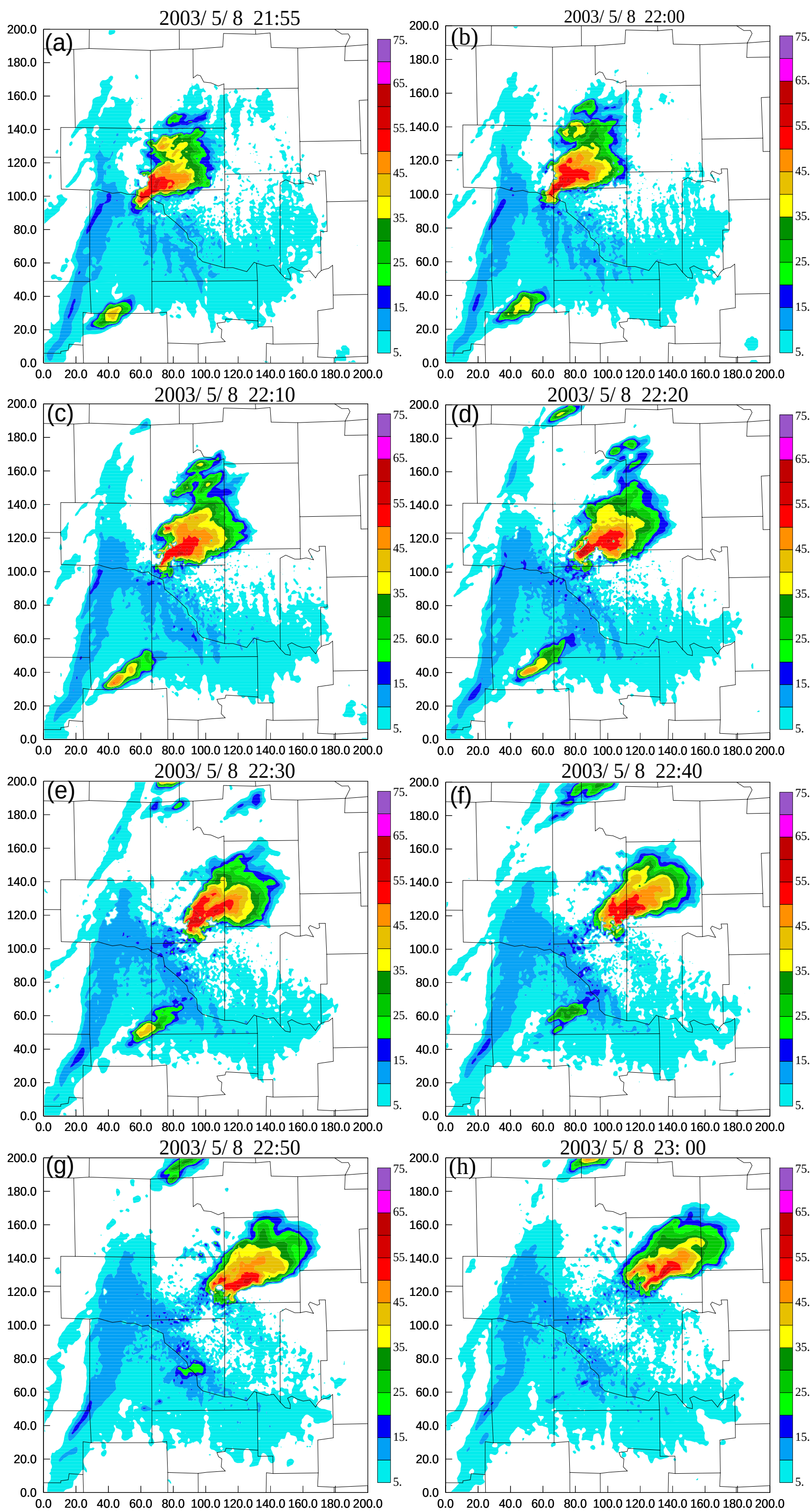

Fig. 4. Reflectivity observed by KTLX radar at the 0.48º elevation at times indicated in the plots.

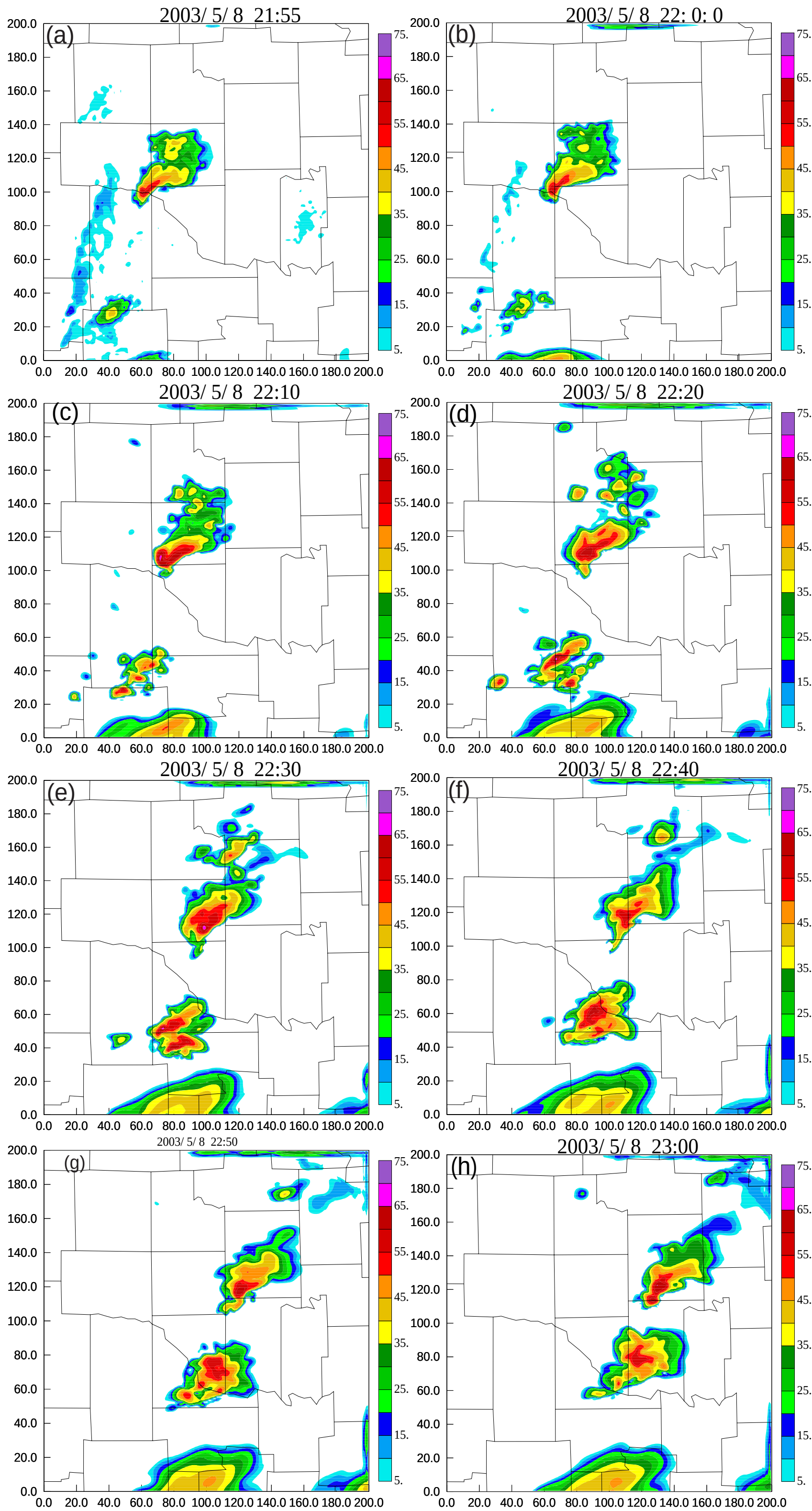

Fig. 5. Ensemble mean analysis reflectivity (a) and ARPS predicted reflectivity at 2200 UTC through 2300 UTC at 10 minute intervals, projected to the 0.48º elevation of the KTLK radar. Both forecasts and analyses were performed at 1 km horizontal resolution. These are the model counterparts of the observed fields shown in Fig. 4.

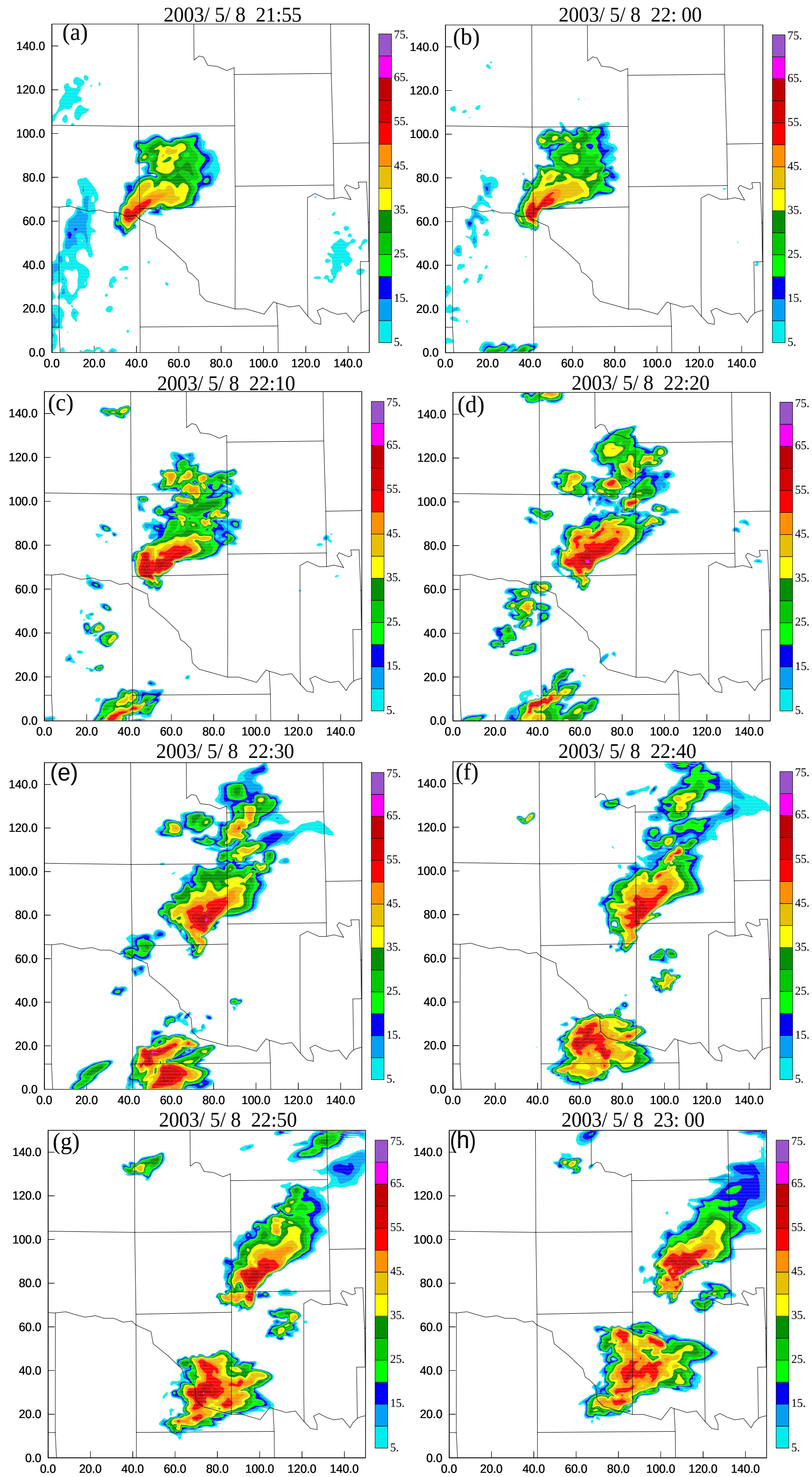

Fig. 6. As Fig. 5 but for forecasts produced at a 500 m horizontal resolution, starting from the 2155 UTC 1 km ensemble mean analysis interpolated to the 500 m grid.

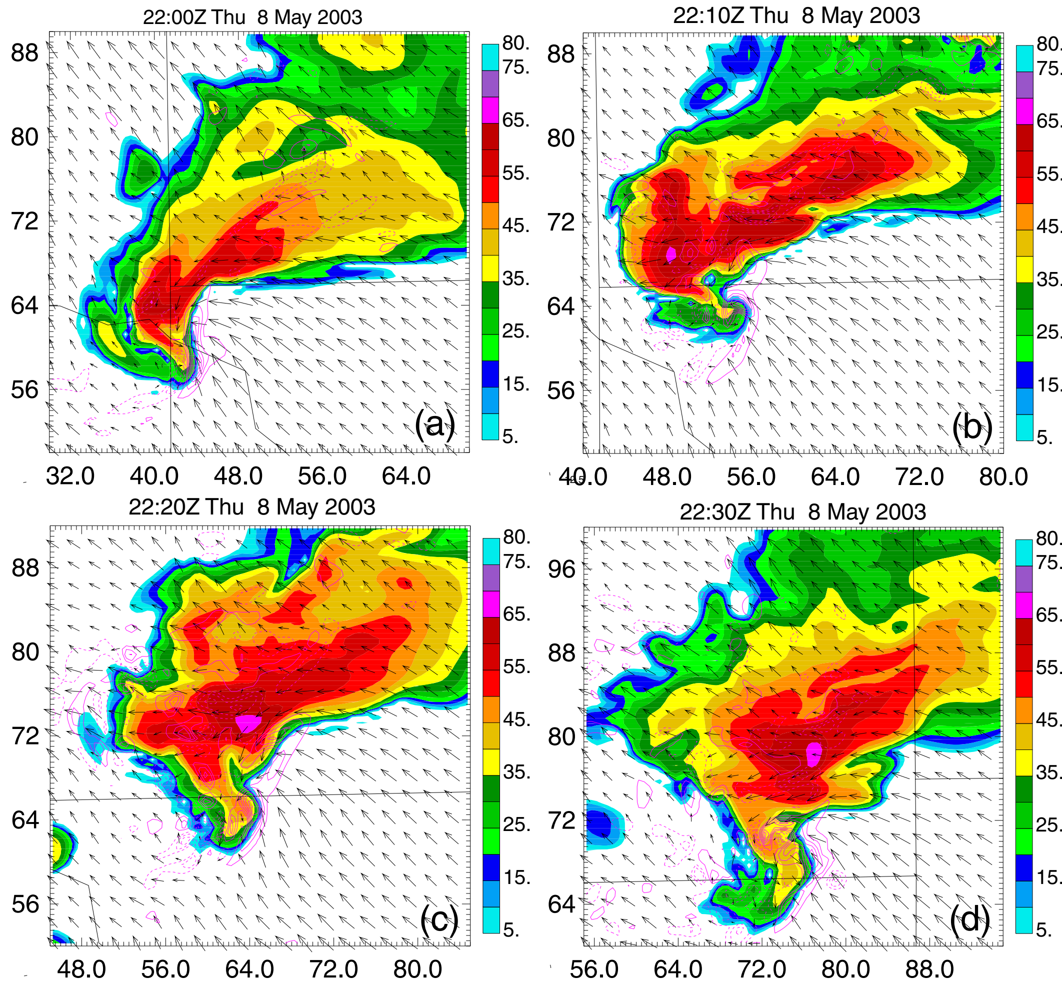

Fig. 7. Forecast reflectivity, wind vector and vertical vorticity at 1 km MSL produced on the 500 m grid, valid at 2200, 2210, 2220 and 2230 UTC. Note that the county map in this figure is incorrectly shifted eastward by about 9 km.

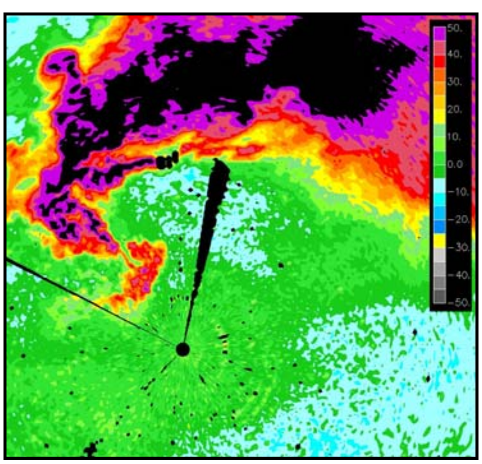

Fig. 8. The 1 degree tilt base reflectivity data from Oklahoma City KOKC TDWR radar at 2208 UTC, 8 May 2003.

On the 500 m grid, the overall storm evolution is similar to that on the 1 km grid, but there are also important differences, especially in the detailed structures of storms. At 2200 UTC, only 5 minutes into the forecast (Fig. 6b), there is already more pronounced hook echo pattern developing in the model than on the 1 km grid, and the reflectivity of the main cell also extends further northeast, in better agreement with the observation (c.f., Fig. 4b). At 2210 UTC, the onset time of the F4 tornado, hook echo with a pin-pointed tip is seen in Fig. 6c, and this hook pattern is maintained for the rest of the forecast.

To see the flow as well as reflectivity structures in the hook echo region more clearly, the 500 m forecast fields at 1 km height level (ground elevation is about 350 m in this area) are plotted in Fig. 7 for the first part of the prediction. It is clear that at all the forecast times shown, there exists a region of strong low-level rotation centering on the northeast side of the reflectivity hook.

Associated with it is strong convergence more or less directed into the rotation center. Such a structure is favorable for low-level rotation through vertical stretching.

At 2210 UTC (Fig. 7b), the reflectivity field shows a narrow ribbon of high reflectivity extending from the main rear-flank reflectivity core towards the southwest, and at its tip an strong localized vorticity maximum is found. Remarkably, very similar structure is found in the low-elevation observation of the Oklahoma City TDWR radar, which is located closer and has a higher sampling resolution that the KTLX observations (Fig. 8). The agreement between the model prediction and the observation down to such fine scale details is extremely encouraging.

4. Summary

In this paper, the results of control experiment for the 8 May 2003 central Oklahoma tornadic supercell storm case, in which a multi-scale EnKF analysis procedure employing two nested grids, are presented. Conventional data, including especially those of Oklahoma Mesonet, are analyzed on the 3 km coarser-resolution grids. The 3 km grid also provided ensemble perturbations representative of mesoscale uncertainty in the storm environment for the nested 1 km storm-sale grid, through both initial perturbations and lateral boundary conditions. Radar together Mesonet data were assimilated on the storm-sale grid every 5 minutes over a 55 minute period. Subsequent forecasts were carried out at 1 km and 500 m horizontal resolutions from the ensemble mean analysis. The forecasts on both grids agree rather well with the observations for the main supercell, capturing well its intensity evolution and its propagation speed and direction. The general hook echo pattern and low-level rotation features are also well captured, with the 500 m solution being even better. In fact, a remarkable agreement is found between the 15-minute forecast on the 500 m grid with the observation of a TDWR radar nearby, down to the fine-scale detail of a thin reflectivity appendage. Such forecasting results appear to be the best that have been obtained so far for a real storm, using EnKF data assimilation method.

A number of sensitivity experiments have been performed. In general, the proper analysis of the storm environment, including the use of mesonet data, is critical for obtaining good forecasts. Additional results will be reported in a full length paper in the future.

Acknowledgement. This work is primarily supported by DPESCOR grant DOD-ONR N00014-06-1-0590, NSF ATM NSF ATM-0530814, and Chinese Natural Science Foundation (CNSF) grant No.40620120437.

References

Anderson, J., 2008: Spatially and temporally varying adaptive covariance inflation for ensemble filters. *Tellus*, **61,** 72 - 83.

Anderson, J. L., 2007: Exploring the need for localization in ensemble data assimilation using a hierarchical ensemble filter. *Physica D: Nonlinear Phenomena*, **230,** 99-111.

Brewster, K., M. Hu, M. Xue, and J. Gao, 2005: Efficient assimilation of radar data at high resolution for short-range numerical weather prediction. *WWRP International Symposium on Nowcasting and Very Short range Forecasting*, CDROM 3.06.

Byun, D. W., 1990: On the analytical solution of flux-profile relationships in the atmospheric surface layer. *J. Appl. Meteor.*, **29,** 652-657.

Dawson, D. T., II, M. Xue, J. A. Milbrandt, and M. K. Yau, 2009: The effects of evaporation and melting in a multi-moment bulk microphysics scheme on the low-level downdrafts and surface cold pools in the simulations of the 3 May 1999 Oklahoma tornadic thunderstorms. *Mon. Wea. Rev.***,** Submitted.

Dong, J., M. Xue, and K. Droegemeier, 2007: The impact of high-resolution surface observations on convective storm analysis with ensemble Kalman filter. *22nd Conf. Wea. Anal. Forecasting/18th Conf. Num. Wea. Pred.*, Salt Lake City, Utah, Amer. Meteor. Soc., CDROM P1.42.

Dowell, D., F. Zhang, L. J. Wicker, C. Snyder, and N. A. Crook, 2004: Wind and temperature retrievals in the 17 May 1981 Arcadia, Oklahoma supercell: Ensemble Kalman filter experiments. *Mon. Wea. Rev.*, **132,** 1982-2005.

Dowell, D. C. and L. J. Wicker, 2004: High-resolution analyses of the 8 May 2003 Oklahoma City storm. Part II: EnKF data assimilation and forecast experiments. *Preprints, 22nd Conf. on Severe Local Storms*, Hyannis, MA,, Amer. Meteor. Soc., CDROM, 12.5.

Dowell, D. C. and L. J. Wicker, 2009: Additive noise for storm-scale ensemble data assimilation *J. Atmos. Ocean. Tech.***,** In press. DOI: 10.1175/2008JTECHA1156.1.

Fujita, T., D. J. Stensrud, and D. C. Dowell, 2007: Surface data assimilation using an ensemble Kalman filter approach with initial condition and model physics uncertainties. *Mon. Wea. Rev.*, **135,** 1846-1868.

Hu, M. and M. Xue, 2007a: Impact of configurations of rapid intermittent assimilation of WSR-88D radar data for the 8 May 2003 Oklahoma City tornadic thunderstorm case. *Mon. Wea. Rev.*, **135,** 507–525.

Hu, M. and M. Xue, 2007b: Analysis and prediction of 8 May 2003 Oklahoma City tornadic thunderstorm and embedded tornado using ARPS with assimilation of WSR-88D radar data. *22nd Conf. Wea. Anal. Forecasting/18th Conf. Num. Wea. Pred.*, Salt Lake City, Utah, Amer. Meteor. Soc., CDROM 1B.4.

Lei, T., M. Xue, T. Yu, and M. Teshiba, 2008: Impact of spatial over-sampling by phased-array radar on convective-storm analysis using ensemble Kalman filter and simulated data. *Symp. Recent Develop. Atmos. Applications Radar Lidar* New Orleans, LA, Amer. Meteor. Soc., P2.17.

Natenberg, E. J. and J. Gao, 2008: Mutiple-Doppler radar analysis of a tornadic thunderstorm using a 3D variational data assimilation technique and ARPS model. *12th Conference on IOAS-AOLS*, Ameri. Meteor. Soc.

Nutter, P., D. Stensrud, and M. Xue, 2004: Effects of coarsely-resolved and temporally-interpolated lateral boundary conditions on the dispersion of limited-area ensemble forecasts. *Mon. Wea. Rev.*, **132,** 2358-2377.

Snook, N. and M. Xue, 2008: Effects of microphysical drop size distribution on tornadogenesis in supercell thunderstorms. *Geophy. Res. Letters*, **35,** L24803, doi:10.1029/2008GL035866.

Snyder, C. and F. Zhang, 2003: Assimilation of simulated Doppler radar observations with an ensemble Kalman filter. *Mon. Wea. Rev.*, **131,** 1663-1677.

Stensrud, D., N. Y. J., D. Dowell, and M. Coniglio, 2008: Assimilating surface data into a mesoscale model ensemble: Cold pool analysis from spring 2007. *Atmos. Res.***,** doi:10.1016/j.atmosres.2008.10.009.

Tong, M., 2006: Ensemble Kalman filer assimilation of Doppler radar data for the initialization and prediction of convective storms, School of Meteorology, University of Oklahoma, 243.

Tong, M. and M. Xue, 2005: Ensemble Kalman filter assimilation of Doppler radar data with a compressible nonhydrostatic model: OSS Experiments. *Mon. Wea. Rev.*, **133,** 1789-1807.

Tong, M. and M. Xue, 2008a: Simultaneous estimation of microphysical parameters and atmospheric state with radar data and ensemble square-root Kalman filter. Part I: Sensitivity analysis and parameter identifiability. *Mon. Wea. Rev.*, **136,** 1630–1648.

Tong, M. and M. Xue, 2008b: Simultaneous estimation of microphysical parameters and atmospheric state with radar data and ensemble square-root Kalman filter. Part II: Parameter estimation experiments. *Mon. Wea. Rev.*, **136,** 1649–1668.

Weisman, M. L. and J. B. Klemp, 1982: The dependence of numerically simulated convective storms on vertical wind shear and buoyancy. *Mon. Wea. Rev.*, **110,** 504-520.

Whitaker, J. S. and T. M. Hamill, 2002: Ensemble data assimilation without perturbed observations. *Mon. Wea. Rev.*, **130,** 1913-1924.

Wicker, L. J. and D. C. Dowell, 2004: High-resolution analyses of the 8 May 2003 Oklahoma City storm. Part III: An ultra-high resolution forecast experiment. *Preprints, 22nd Conf. Severe Local Storms,*, Hyannis, MA, Amer. Meteor. Soc., CDROM, 12.6.

Xue, M., M. Tong, and K. K. Droegemeier, 2006: An OSSE framework based on the ensemble square-root Kalman filter for evaluating impact of data from radar networks on thunderstorm analysis and forecast. *J. Atmos. Ocean Tech.*, **23,** 46–66.

Xue, M., D.-H. Wang, J.-D. Gao, K. Brewster, and K. K. Droegemeier, 2003: The Advanced Regional Prediction System (ARPS), storm-scale numerical weather prediction and data assimilation. *Meteor. Atmos. Physics*, **82,** 139-170.

Xue, M., K. K. Droegemeier, V. Wong, A. Shapiro, K. Brewster, F. Carr, D. Weber, Y. Liu, and D.-H. Wang, 2001: The Advanced Regional Prediction System (ARPS) - A multiscale nonhydrostatic atmospheric simulation and prediction tool. Part II: Model physics and applications. *Meteor. Atmos. Phy.*, **76,** 143-165.

Zhang, F., C. Snyder, and J. Sun, 2004: Impacts of initial estimate and observations on the convective-scale data assimilation with an ensemble Kalman filter. *Mon. Wea. Rev.*, **132,** 1238-1253.